JMEPEG
https://doi.org/10.1007/s11665-026-13709-1


1059-9495/$19.00

ORIGINAL RESEARCH ARTICLE

# Anti-Corrosion Epoxy Coating Enhanced by the Modified Boron Nitride Coupled with Ce-MOF

*Yanqiu Zhang, Hongwei Zhao, Zhaowen Tian, Ruiyu Ma, Zheyan Tang, Lixiang Li, Qingdong Li, Xueyuan Zhang, and Baigang An*

Submitted: 18 November 2025 / Revised: 12 February 2026 / Accepted: 23 February 2026

**Both boron nitride (BN) and metal-organic framework (MOF) are ideal nanofillers to enlarge corrosion resistance of coating due to their two-dimensional layered or porous structure with special physical-chemical property. However, the agglomeration and weak interaction with epoxy resin (EP) blocks their effects on enhancing anticorrosion performance of EP coatings. In this work, BN was hydroxylated and subsequently coated with polydopamine (PDA), then onto which cerium metal-organic frameworks (Ce-MOFs) was in-situ grown to get BNOH@PDA-Ce-MOFs. This technology not only ensures good dispersibility of BN and Ce-MOF, but strengthens their interaction with EP through PDA modified layer. BN uniformly dispersed in EP can elongate the diffusion path of corrosive media to enhance the barrier properties of the coating. Meanwhile, Ce-MOF can form a dense passivation layer composed of hydroxide and oxides of cerium to further protect the metal from corrosion. Therefore, the electrochemical impedance spectroscopy (EIS) measured $|Z|_{0.01\ Hz}$ value of BNOH@PDA-Ce-MOFs/EP coating only relatively decreased after 56 days, remaining three orders of magnitude higher than that of pure EP coatings. Moreover, the accelerated salt spray test of 28 days, there are no obvious corrosion pits, confirming the excellent corrosion resistance of BNOH@PDA-Ce-MOFs/EP coating.**

**Keywords** boron nitride, cerium metal-organic frameworks, corrosion, polydopamine

## 1. Introduction

Corrosion of metals results in significant financial losses and poses severe threats to the safety of industrial equipment such as marine facilities, ships, and buildings. Consequently, the issue of metal corrosion has attracted widespread attention in the world (Ref 1-3). Applying organic coatings onto metal is a straightforward, effective, and cost-efficient method to prevent them from corrosion (Ref 4-6). Epoxy resin (EP) coatings exhibit excellent heat and chemical resistance, as well as robust physical and mechanical properties, which can also provide an effective barrier against corrosive media (Ref 7-9). Nevertheless, some defects and micro-cracks are inevitably formed in the EP coatings during the curing process and subsequent usage, which allows the corrosive medium to transport toward the metal substrate (Ref 10, 11). Therefore, optimizing the barrier properties of EP coatings to enhance their corrosion resistance is imperative.

Two-dimensional (2D) materials such as graphene/graphene oxides have been used as nanofillers to enhance the impermeability properties of EP coatings, due to their high physical aspect ratio, excellent barrier properties, and exceptional chemical stability (Ref 12-14). As the surface of graphene oxides are rich in functional groups including hydroxyl and carboxyl, they are readily to be filled and dispersed into EP. However, the high electrical conductivity of graphene/graphene oxides can induce a galvanic cell effect upon connected with the metal substrate, potentially accelerating corrosion of metals if the coating was damaged (Ref 15-17). Boron nitride (BN) offers a promising alternative to graphene. BN possesses a 2D structure similar to graphene and exhibits superior barrier properties, mechanical strength, hydrophobicity, abrasion resistance, and thermal conductivity (Ref 18-20). However, the inert BNs tend to aggregate in polymer matrix, the dispersion of BN in EP remains a critical bottleneck limiting the further application of BN in anticorrosive coatings. Surface functionalization of BN is considered as an effective strategy to improve the dispersion of BN in solvents and polymers. For example, Wu et al. added the polyethyleneimine grafted BN into EP, the barrier property and anticorrosion ability of the coating was significantly improved (Ref 21). This enhancement can be attributed to the BN nanosheets' physical barrier effects and the crosslinking action of poly-ethyleneimine on the EP. Similarly, BN modified with polydopamine (PDA) can adjust its electronic structure and interfacial energy, thereby enhancing its dispersion within polymer matrices (Ref 22). Nevertheless,

**Supplementary Information** The online version contains supplementary material available at https://doi.org/10.1007/s11665-026-13709-1.

**Yanqiu Zhang, Hongwei Zhao, Zhaowen Tian, Ruiyu Ma, Zheyan Tang,** and **Lixiang Li**, Key Laboratory of Energy Materials and Electrochemistry Liaoning Province, School of Chemical Engineering, University of Science and Technology Liaoning, Anshan 114051, China; **Qingdong Li** and **Xueyuan Zhang**, Institute of Corrosion Science and Technology, Guangzhou 510530, China; and **Baigang An**, Key Laboratory of Energy Materials and Electrochemistry Liaoning Province, School of Chemical Engineering, University of Science and Technology Liaoning, Anshan 114051, China; and Institute of Corrosion Science and Technology, Guangzhou 510530, China. Contact e-mails: lxli2005@126.com and bgan@ustl.edu.cn.



Published online: 28 March 2026

only physical barrier is far from requirements for coatings with good anticorrosion property.

Adding corrosion inhibitors into EP coatings can significantly enhance their anticorrosive properties. Cerium metal-organic frameworks (Ce-MOFs) have recently emerged as promising nanoscale corrosion inhibitors (Ref 23-26). For instance, Motamedi et al. synthesized a new type of cerium-based MOF and investigated its effects on the corrosion resistance of EP coatings (Ref 27). The results showed that the Ce-MOF modified EP coating exhibited excellent barrier protection and self-healing capabilities. Zhao et al. developed the dual-functional Ce-MOF/carbon fiber composites by using in situ growth techniques, which was used as the filler to significantly improve the permeation resistance and corrosion protection of the EP coatings (Ref 23). The corrosion inhibition involves the formation of a cerium hydroxide/oxide passivation film that physically isolates the metal surface from the corrosive electrolyte, thereby preventing further corrosion (Ref 28, 29). Meanwhile, the 2-methylimidazole ligands in Ce-MOFs can catalyze the ring-opening polymerization of epoxy resin (EP), which increases the crosslinking density and interfacial compatibility within the EP matrix (Ref 30-32). Does it bring more anticorrosion properties, if an effective combination of BN and MOF in EP coatings were achieved to play synergistic effects on corrosion inhibition?

Herein, we proposed a strategy combining layer-by-layer self-assembly and interface coordination growth to construct a multi-level structure of BNOH@PDA-Ce-MOFs composite filler for anticorrosion coating, aiming to overcome the limitations of weak interface bonding and single functionality of inert fillers. BNOH@PDA-Ce-MOFs consists of the hydroxyl-modified BN (BNOH) covered by a uniform polydopamine (PDA) adhesive layer via hydrogen bonding, on which a dense cerium-based metal-organic frameworks (Ce-MOFs) layer was in situ grown through the coordination chelation of $Ce^{3+}$ with the catechol groups in PDA. This design is expected to achieve excellent dispersion of filler in epoxy matrix through strong interfacial adhesion of PDA and synergistic effect of 2-methylimidazole. Meanwhile, the incorporated Ce-MOFs provides corrosion inhibition of the coating. The present study provides a novel filler functionalization design concept towards high-performance anti-corrosion coatings.

## 2. Experimental

### 2.1 Chemicals and Reagents

Boron nitrides (BN, 5-10 $\mu$m) were purchased from Anhui Zesheng Technology Co. Ltd. Nitric acid ($HNO_3$, 65.0-68.0%), methanol (MeOH, 99.5%), and ethanol (EtOH, 99.5%) were bought from Sinopharm chemical reagent. Tris(hydroxymethyl)aminomethane (Tris, 99.9%), dopamine hydrochloride (DA, 98%), cerium nitrate hexahydrate ($Ce(NO_3)_3{\cdot}6H_2O$, 99.5%), and 2-methylimidazole (2-MI, 98%) were provided by Aladdin. Bisphenol epoxy resin (EP, Standard number: Q/320601NHS601) was bought from Nantong Xingchen Synthetic Material Co., Ltd. Polyamide resin (Enforce standards: Q/DBSZ 01-2022) was got from Dingyuan resin Co., Ltd. The Q235 steel sheets with 40 × 20 × 2 mm coated with coatings were used as electrodes for the electrochemical measurements and salt spray tests.

### 2.2 Synthesis of BNOH@PDA and BNOH@PDA-Ce-MOFs

The synthesis process and detailed steps of fillers and intermediates are shown in Fig. 1. BN of 10.0 g and concentrated $HNO_3$ (5 mol·$L^{-1}$) of 200 mL were put into a hydrothermal reactor. The hydrothermal reaction was carried out at 90 °C for 3 h in an autoclave, then it was cooled down to room temperature, followed by deionized water washing until neutral and drying at 60 °C for 12 h in air to obtain hydroxylated boron nitride (BNOH).

Tris(hydroxymethyl)aminomethane (Tris) of 5.0 g was dissolved in 2 L deionized water, the pH value of solution was adjusted to 8.5 by 0.1 mol·$L^{-1}$ HCl, followed by the addition of 5.0 g BNOH. The mixture was stirred for 30 min, then dopamine hydrochloride (DA) of 5.0 g was added into and the solution accompanying with continuously stir for an additional 24 h. Subsequently, the mixture was washed with deionized water and centrifuged three times to remove separately polymerized DA. The product was dried and named BNOH@PDA.

A total of 5.0 g of BNOH@PDA and 5.0 g of $Ce(NO_3)_3{\cdot}6H_2O$ were added into 200 mL methanol (MeOH) and stirred thoroughly, which was labeled as Solution A. 2.5 g of 2-methylimidazole was completely dissolved in 200 mL MeOH, which was labeled as Solution B. Then Solution A and Solution B were mixed at room temperature with stirring for 4 h. The resulted mixture was then washed three times by MeOH, dried at 60 °C for 12 h under ambient conditions to BNOH@PDA-Ce-MOFs. For the sake of comparing samples, BN-Ce-MOFs and BNOH-Ce-MOFs were also prepared under the conditions similar to BNOH@PDA-Ce-MOFs.

### 2.3 Fabrication of Coatings

20.0 g epoxy resin (EP) was uniformly dispersed in 20.0 mL EtOH, then 0.4 g of BNOH@PDA-Ce-MOFs were added into the solution accompanying with stir for 4 h. Then, 20.0 g curing agent was introduced into the solution with a continuously mixing of 0.5 h to form a uniform EP slurry containing BNOH@PDA-Ce-MOFs, which was coated on the carbon steel sheet and then to be solidified at room temperature for 24 h, followed by drying at 60 °C for 12 h in air to obtain the composite coating, designated as BNOH@PDA-Ce-MOFs/EP. The other epoxy composite coatings were prepared by using similar methods, including pure EP, BN/EP, and BNOH@PDA/EP coatings. The thickness of all coatings was controlled to 50 ± 5 $\mu$m.

### 2.4 Materials Characterizations

Surface morphologies and element distribution of samples were performed by scanning electron microscopy (SEM, Apreos, FEI, USA) with the 10 kV accelerating voltage. The crystal patterns of samples were analyzed by wide-angle X-ray diffraction test (XRD, D8 ADVANCE, Bruker, Germany) with Cu Kα irradiation (λ = 0.15406 nm) in the range of 2θ from 10 to 90°. The chemical structures of samples were studied by a Fourier transformed infrared spectrometer (FT-IR, EQUINOX55, Bruker, Germany) in the wavenumber range of 4000-400 $cm^{-1}$. The chemical states of samples were analyzed by X-ray photoelectron spectroscopy (XPS, AXIS-SUPRA,

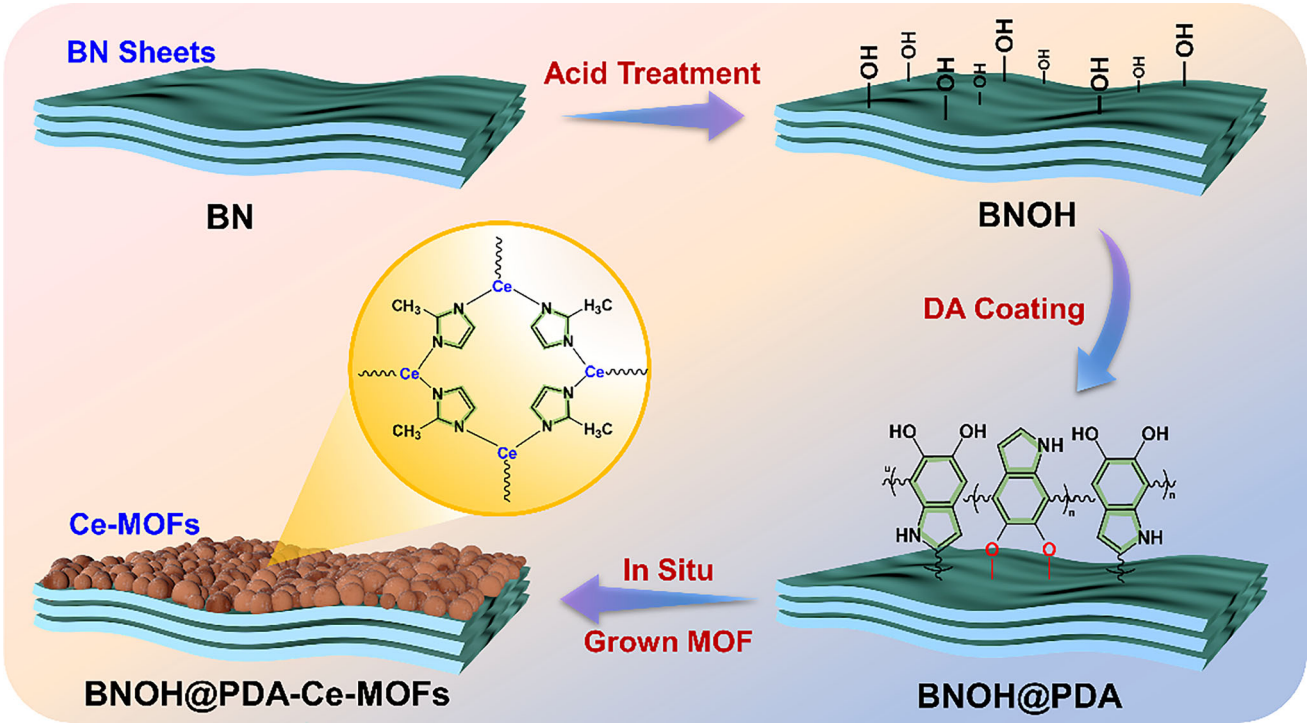


**Fig. 1** Schematic illustration of the preparation of BNOH@PDA-Ce-MOFs composites

Supra, Japan) by using Al Kα radiation (1486.6 eV) as the exciting source. The resulting spectra were corrected by C 1s line at 284.6 eV.

The corrosion resistance of the coatings was evaluated by electrochemical impedance spectroscopy (EIS) and neutral salt spray tests. In a three-electrode system, the coated steel, the platinum plate with a surface area of 1 $cm^2$, and an Ag/AgCl electrode were used as working electrode, counter electrode, and reference electrode. The EIS was carried out by an electrochemical workstation (Gamry Interface 1010E) over the frequency from 0.01 Hz to 100 kHz with an amplitude of 10 mV at room temperature. To evaluate the corrosion resistance performance of coatings, salt spray tests were conducted under the conditions of 5 wt.% NaCl solution and continuous spraying at 35 °C for 672 h. Finally, the morphology of samples was analyzed by optical microscope (YM710TR, YueScope). The adhesion of the coating was measured by a pull-off adhesion tester (Posi Test AT-A, Deflsko, America) before and after immersing in 5.0 wt.% NaCl solution for 7 days. At least three parallel samples under same condition were tested to ensure the reproducibility of results.

## 3. Results and Discussion

The SEM images of samples are shown in Fig. 2. The pristine BN has a typical lamellar morphology. After hydroxylation and PDA modification, the resulted BNOH@PDA retains a lamellar feature similar to BN. Hereafter, Ce-MOFs were successfully grown on the surface of BNOH@PDA to get BNOH@PDA-Ce-MOFs by an interfacial induction strategy, the product still maintains an intact layered structure, confirming that the preparation process effectively preserves the intrinsic structure of BN matrix. EDS elemental mapping shown in Fig. 2g demonstrates that the Ce element is uniformly distributed in BNOH@PDA-Ce-MOFs, indicating the uniform deposition of Ce-MOFs. Moreover, in Fig. 2e-f, the STEM images of BNOH@PDA-Ce-MOFs clearly show the PDA layer and Ce-MOFs on the BN surface. In contrast, pure BN and BNOH lack dopamine-derived catechol functional groups, and thus cannot achieve uniform deposition of Ce-MOF (Fig. S1 and S2). The results suggest that hydroxylation and PDA interfacial modification on the BN is an effective approach to enhance the interaction of Ce-MOFs with BN.

The crystal structures of samples were analyzed by using XRD spectra (Fig. 3a). The BN displays the diffraction peaks at 26.7, 41.5, 50.3, and 55.2°, corresponding to the (002), (100), (102), and (004) crystal planes of BN (JCPDS 34-0421) (Ref 33, 34) respectively. The materials after hydroxylation and PDA modification still maintain the crystalline structure of BN. The Ce-MOFs deposition results the wide peaks of $CeO_2$ at 28.5, 47.3, and 56.3°. Besides the diffraction peaks of $CeO_2$ and BN, no other peaks are detected in BNOH@PDA-Ce-MOFs, inferring that Ce-MOFs is an amorphous structure (Ref 32).

The functional groups of samples were characterized by FT-IR spectrum. In Fig. 3b, the absorption peaks of BN at 781 and 1360 $cm^{-1}$ correspond to B-N bonds (Ref 9). Compared to BN, BNOH@PDA and BNOH@PDA-Ce-MOFs display new absorption bands (C=C/C–N, Ce–N, C=N). For the BNOH@PDA, an additional absorption peak at 1628 $cm^{-1}$ assigned to the benzene ring structure of PDA can be observed (Ref 35), indicating that BN has been successfully modified by PDA. Notably, the characteristic peaks of C=N (1036 $cm^{-1}$), Ce–N (1463 $cm^{-1}$), and C=C/C–N (1628 $cm^{-1}$) bonds further confirm the presence of Ce-MOFs in the BNOH@PDA-Ce-MOFs (Ref 27). The appearance of these features confirms the successful assembly of Ce-MOFs on the surface and implies interfacial bonding via the PDA bridge.

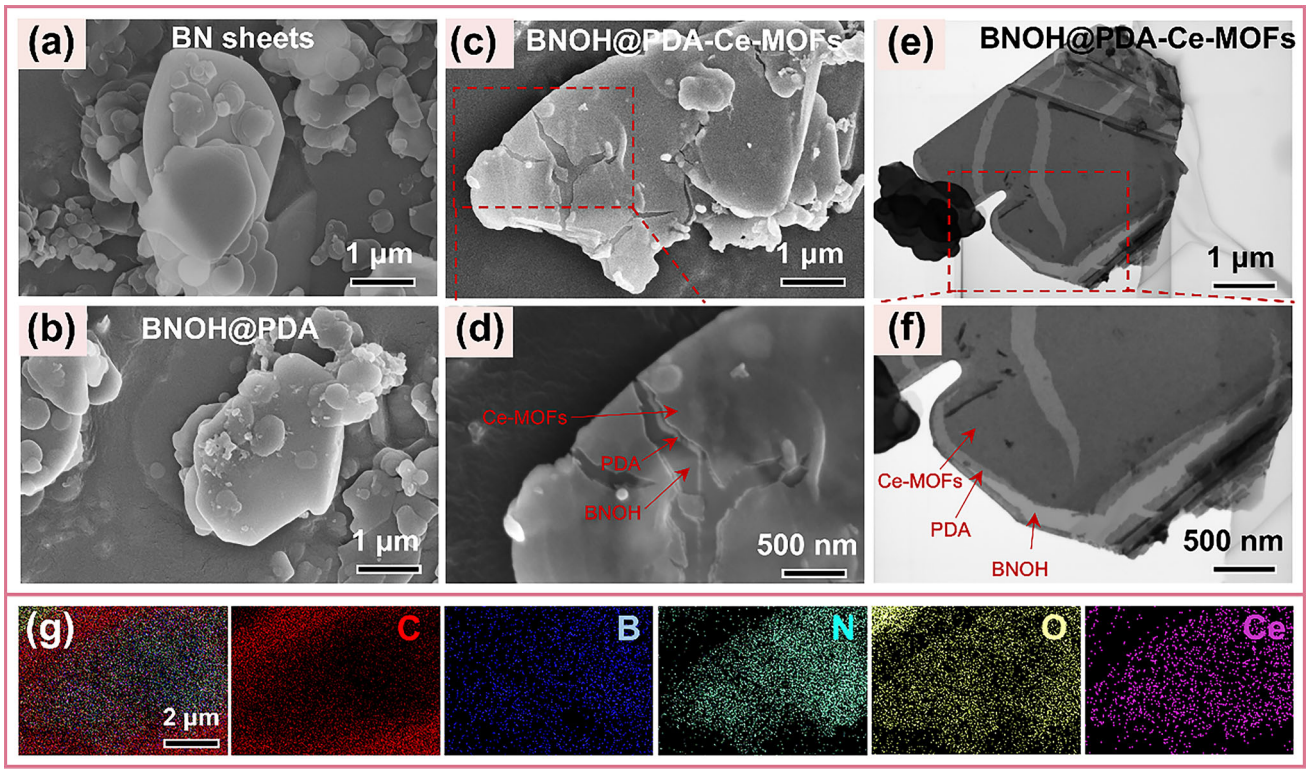


**Fig. 2** SEM images of (a) BN and (b) BNOH@PDA. (c) BNOH@PDA-Ce-MOFs and (g) corresponding EDS mappings containing C, B, N, O, Ce elements. (d) SEM images of BNOH@PDA-Ce-MOFs with high magnification. (e-f) STEM images of BNOH@PDA-Ce-MOFs

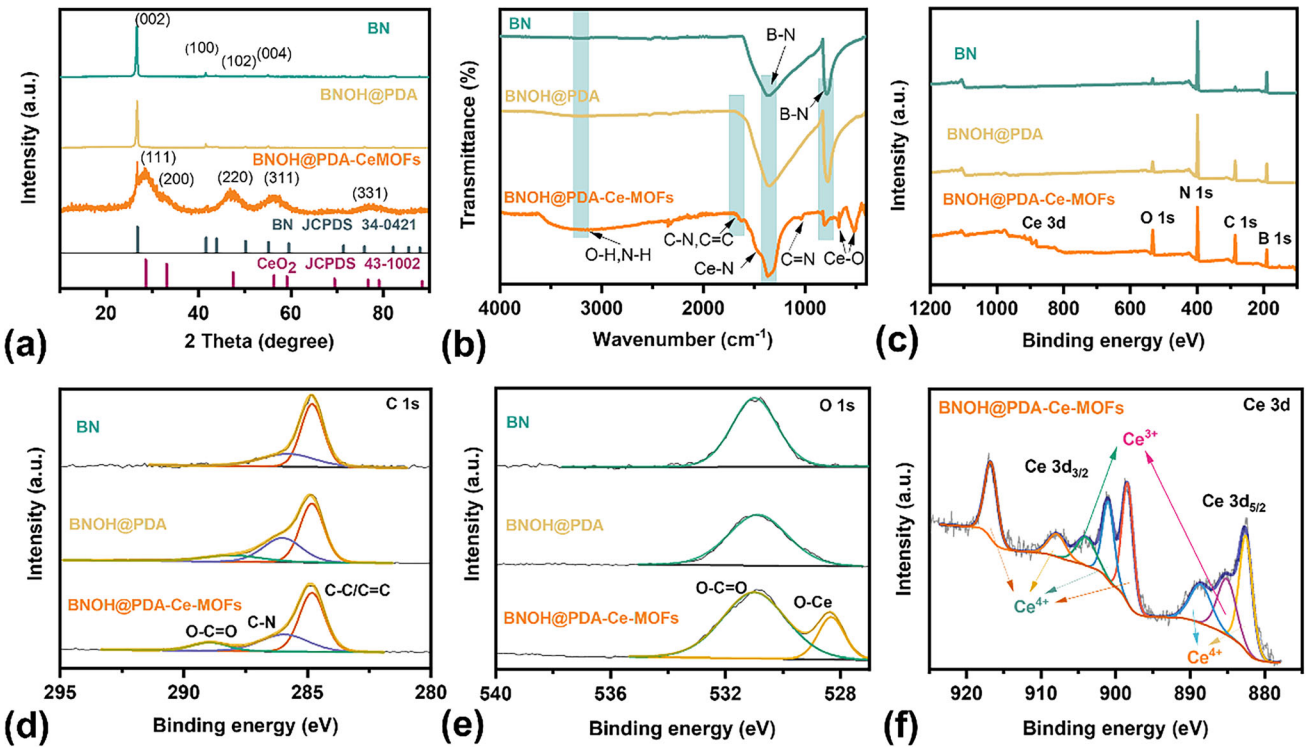


**Fig. 3** The composition and chemical states of samples: (a) XRD patterns, (b) FT-IR curves, (c) XPS survey spectra, (d-e) high-resolution XPS spectra of C 1s and O 1s, respectively. (f) The high-resolution XPS spectra of Ce 3d of BNOH@PDA-Ce-MOFs

The elemental composition and chemical state of samples were investigated by the XPS analysis. In Fig. 3c, the characteristic peaks of B 1s and N 1s were clearly observed in wide spectrum for BN. Notably, the intensity of C 1s peak increases in BNOH@PDA, attributing to the introduction of PDA. For BNOH@PDA-Ce-MOFs, a distinct Ce 3d peak

appears, suggesting that the Ce-MOFs have been grafted on BNOH@PDA. As shown in high-resolution C 1s spectra (Fig. 3d), the C–N (286.0 eV) intensity in BNOH@PDA and BNOH@PDA-Ce-MOFs has become stronger compared with BN, and an additional O–C=O (288.4 eV) peak has been fitted. These changes can be attributing to the effects of PDA and 2-methylimidazole (Ref 36). In the O 1s high-resolution spectra (Fig. 3e), an additional O–Ce (529.1 eV) bond can be observed in BNOH@PDA-Ce-MOFs compared with BNOH@PDA, which can be attributed to the byproduct $CeO_2$ and the interaction between metal ions and catechol groups from PDA (Ref 24). Fig. 3f shows the high-resolution Ce 3d spectra, where the Ce $3d_{5/2}$ peaks are located at 888.5 eV and 882.2 eV, and the Ce $3d_{3/2}$ peaks are located at 898.1 and 916.2 eV, confirming the coexistence of $Ce^{4+}$ and $Ce^{3+}$ in BN@PDA-Ce-MOFs (Ref 37, 38). Notably, the characteristics of Ce-MOFs in the BNOH@PDA-Ce-MOFs composite surface are consistent with those of the pure Ce-MOF material (Fig S3).

As shown in Fig. S4a and b, all the isotherms of samples (Fig. S4a) exhibited a rapid $N_2$ adsorption occurring at $P/P^0 > 0.9$, which confirms the presence of a certain amount of mesopores. In contrast, BNOH@PDA-Ce-MOFs possesses the larger adsorption capacity than BN and BNOH@PDA, suggesting its high specific surface area. Meanwhile, Fig. S4b shows that BNOH@PDA-Ce-MOFs contains an increased population of small mesopores compared with the other samples except Ce-MOFs. The larger specific surface area and pore volume of BNOH@PDA-Ce-MOFs are expected to provide abundant active sites for interfacial bonding with the EP.

As the nanofiller, BN, BNOH@PDA, and BNOH@PDA-Ce-MOFs were respectively filled in EP. Fig. S5 showed that the unmodified BN aggregates extensively in epoxy matrix, while the modified BN (BNOH@PDA and BNOH@PDA-Ce-MOFs) can be uniformly dispersed in epoxy matrix. Consequently, the corresponding composite coatings were prepared by adding the curing agent, and morphology of the coatings was analyzed by SEM. As shown in Fig. 4a and b, the cross-sections of EP and BN/EP composite coatings exhibit typical brittle fracture, there are many holes and cracks (Fig. S6a). After PDA modification, the number of defects in the BNOH@PDA/EP coating decrease significantly (Fig. 4c and S6c), which can be attributed to the effective improvement of BN dispersion by interfacial modification of PDA (Ref 35). Notably, the BNOH@PDA-Ce-MOFs/EP coating displays a more uniform and compact surface (Fig. 4d) due to that the 2-methylimidazole ligand in Ce-MOFs promotes the ring-opening polymerization of epoxy groups (Ref 32), synergistically enhancing the chemical bonding interaction between the filler and the epoxy resin matrix with the assistance of PDA. The distribution of N, B, and Ce elements in the BNOH@PDA-Ce-MOFs/EP shown in Fig. 4e illustrates that N, B, and Ce elements are uniformly distributed in the composite coating, which further verifies the excellent dispersibility of BNOH@PDA-Ce-MOFs composite materials in EP. The results demonstrate that PDA and Ce-MOFs modification on BN not only improves the uniform dispersion of the filler but also promotes the formation of a highly compact physical barrier network in the coating, therefore it could be expected to bring the coating good anticorrosion performance.

Electrochemical impedance spectroscopy (EIS) was firstly employed to assess the corrosion resistance of materials (Ref 39). Fig. 5a-h present the Bode plots of coatings, and the corresponding Nyquist plots shown in Fig. S8. Generally, a higher |Z| value at 0.01 Hz ($|Z|_{0.01\ Hz}$) in the Bode-modulus plots and a larger capacitive arc radius in the Nyquist plot represent the superior corrosion resistance of the coatings. As shown in Fig. 5a, the initial $|Z|_{0.01\ Hz}$ value of the EP coating is $1.36 \times 10^7\ \Omega{\cdot}cm^2$. However, when the immersion time extended to 56 days, $|Z|_{0.01\ Hz}$ value significantly decreased by two orders of magnitude to $8.24 \times 10^4\ \Omega{\cdot}cm^2$, and the corresponding capacitive arc radius in the Nyquist plot also markedly decrease (Fig. S8a). During the early immersion stage (1 day), Bode-phase plots reveal a single time-constant. When the immersion time reached 14 days, the plots represent two time-constants feature (Fig. 5e). This is primarily due to that corrosive medium penetrate from the inherent defects and micro-cracks of EP coating to reach the surface of the Q235 steel substrate. As the barrier properties of EP coating deteriorate, the electrochemical corrosion reaction of the metal matrix is triggered. In contrast, the EP with BN fillers results the coating a moderate enhancement in corrosion resistance. As shown in Fig. 5b, a relatively slow decrease in the $|Z|_{0.01\ Hz}$ value that declines from an initial value of $1.27 \times 10^8\ \Omega{\cdot}cm^2$ to $3.56 \times 10^6\ \Omega{\cdot}cm^2$ during 56 days immersion. Bode-phase plots maintain a single time-constant characteristic up to 28 days of immersion (Fig. 5f). Meanwhile, the radius of the capacitive arc in the Nyquist plot still exhibits a significant decreasing trend (Fig. S8b).

The coatings filled with BNOH@PDA or BNOH@PDA-Ce-MOFs (Fig. 5c and d) exhibit significantly improved corrosion resistance, with $|Z|_{0.01\ Hz}$ value of $4.62 \times 10^7\ \Omega{\cdot}cm^2$ and $1.27 \times 10^8\ \Omega{\cdot}cm^2$ after 56 days of immersion, which outperforms the value of 2-3 magnitudes, comparing with that of pure EP and BN/EP coatings. Especially, the introduction of Ce-MOFs enables the coating the better anticorrosion property. Correspondingly, the $|Z|_{0.01\ Hz}$ values of Ce-MOFs/EP coating decreased from $3.13 \times 10^8$ to $1.33 \times 10^7\ \Omega{\cdot}cm^2$ after 56 days immersion as shown in Fig. S7 and Table S1. Compared with other samples reported in this work, the Ce-MOFs/EP coating exhibited obviously superior corrosion protection to the pure EP and BN/EP coatings, although its performance was relatively inferior to that of BNOH@PDA/EP and BNOH@PDA-Ce-MOFs/EP coatings. The results confirm that as a filler, Ce-MOF can also effectively enhance the corrosion resistance of epoxy coating. The enhanced corrosion resistance could be attributed to two key factors. The synergistic effect of PDA and 2-methylimidazole optimizes the dispersion stability of BN fillers to enhance the physical barrier properties of the coating. On the other hand, a dense passivation layer of $Ce(OH)_3/CeO_2$ could be formed on the metal matrix when corrosion medium penetrate into the coating, which can protect the metal matrix from corrosion. Notably, the $|Z|_{0.01\ Hz}$ value of BNOH@PDA-Ce-MOFs/EP coating remains consistently higher than the other coatings across all immersion stages (Fig. 5i), demonstrating its superior long-term anticorrosion performance. As shown in Fig. S9, to be compared with the functional coatings, the properties by comparing the $|Z|_{0.01\ Hz}$ value of coatings, anticorrosion property of BNOH@PDA-Ce-MOFs coating is superior to those materials recently reported (Ref 7, 8, 16, 21, 39-42).

As shown in Fig. S8, as immersion time prolonged, obvious changes can be discerned from the configuration of EIS of samples. The pure EP coatings whose loops in the high-frequency of EIS quickly decrease with immersion time, indicating the coatings are easy to be penetrated. Moreover, the

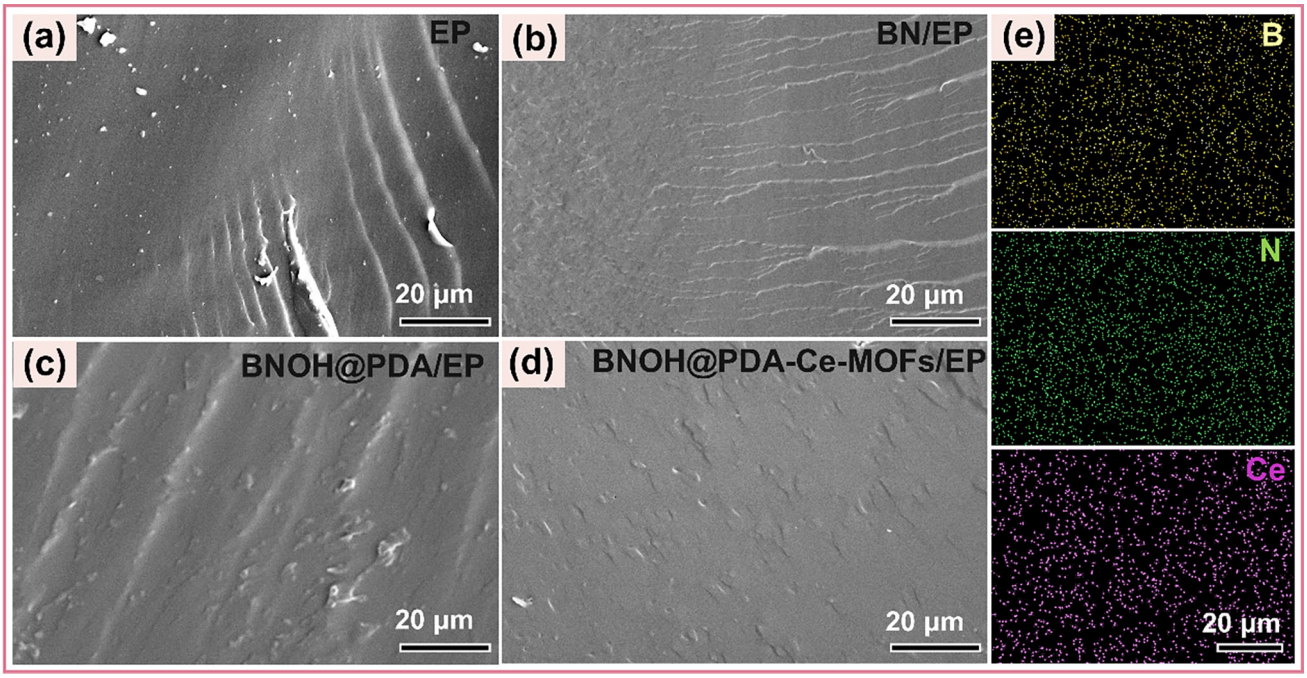


**Fig. 4** Cross-sectional SEM images of coatings: (a) EP, (b) BN/EP, (c) BNOH@PDA/EP, and (d) BNOH@PDA-Ce-MOFs/EP coating. (e) The corresponding EDS mappings

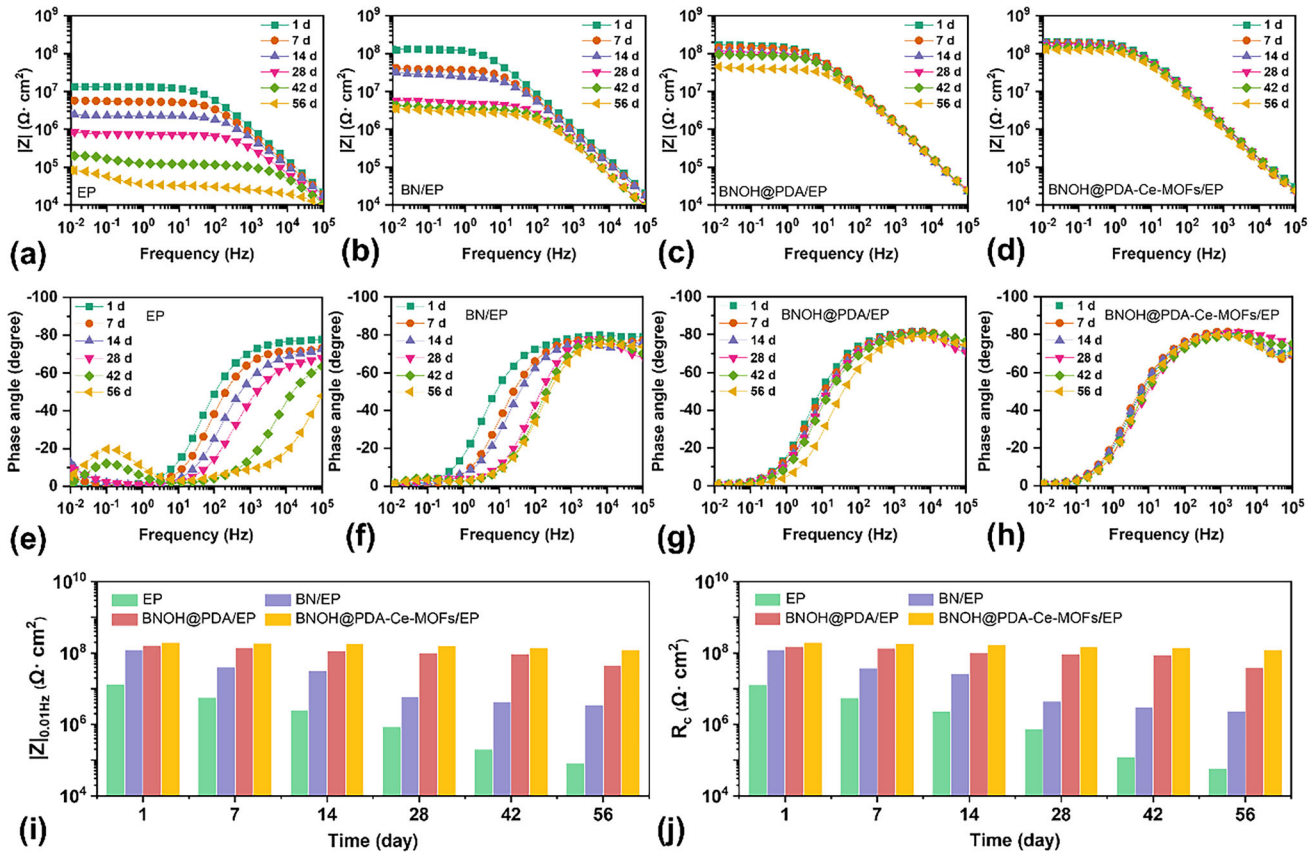


**Fig. 5** The Bode-modulus plots of (a) EP, (b) BN/EP, (c) BNOH@PDA/EP, (d) BNOH@PDA-Ce-MOFs/EP coatings immersed in 3.5 wt.% NaCl solution and corresponding Bode-phase plots (e-h, respectively). (i) Evolution of $|Z|_{f=0.01\ Hz}$ values. (j) Evolution of Rc values

inductive loop that is an indicative of local corrosion of metal matrix appears after 42 days immersion. However, such an inductive loop can not be observed even after 56 days immersion for BNOH@PDA-Ce-MOFs/EP coating. Meanwhile, the amplitude of loop diameter remains in a magnitude with a small change for BNOH@PDA-Ce-MOFs/EP coating

comparing with the other coatings, attributing to its good anticorrosion property.

The equivalent circuit models corresponding to Nyquist plots of Fig. S8 are shown in Fig. S10, which was used to fit EIS to get the parameters related to the anticorrosion properties of coatings. In the equivalent circuit model, $R_s$, $R_c$, and $R_{ct}$ represent solution resistance, coating resistance, and charge transfer resistance, respectively. $Q_c$ and $Q_{dl}$ were denoted as coating capacitance and double-layer capacitance, respectively. Among these parameters, $R_c$ is one of the key indicators reflecting the porosity of the coating (Ref 43). According to the parameters listed in Table S1, after an immersion test of 56 days, $R_c$ value of the BNOH@PDA-Ce-MOFs/EP coating only decreases from an initial value of $1.97 \times 10^8$ $\Omega \cdot cm^2$ to $1.22 \times 10^8$ $\Omega \cdot cm^2$ and maintains the highest $R_c$ value at each immersion stage (Fig. 5j) comparing with the other coatings. Furthermore, quantitative comparison of water uptake behavior can also reflect porosity and barrier properties of coatings. The water uptake ratios of coating calculated using the equation: $w_{uptake} = \frac{m_t - m_0}{m_0} \times 100\%$, where $m_0$ and $m_t$ represent the mass of coating before and after being immersed in a 3.5 wt.% NaCl solution for t hours, respectively. As shown in Fig. S11, after 480 hours of immersion, the $w_{uptake}$ of BNOH@PDA-Ce-MOFs/EP coating is 0.9% and lower than that of the other coatings, demonstrating excellent long-term corrosion resistance. The results can be attributed to the more uniform dispersion of BN in the EP matrix after modification with PDA and 2-methylimidazole, which effectively suppresses the formation of pores and interfacial defects in the coating.

The corrosion resistance of coatings under harsh conditions was evaluated through neutral salt spray tests. Fig. 6 and S12 show the visual images of coatings exposed to 5.0 wt.% NaCl salt spray for 7, 14, 21, and 28 days. For the pure EP coating (Fig. 6a and S12a), obvious bubbles and corrosion pits appeared on the steel surface after 7 days of exposure. As the exposure time increased, the corrosion becomes more seriously due to the penetration of corrosive media to the substrate surface through defects and pores of the coating. After the introduction of BN, the BN/EP coating exhibits superior corrosion resistance compared to the pure EP coating during the initial salt spray exposure period (Fig. 6b and S12b). However, after 28 days of exposure, the corrosion level remained relatively severe. It is attributed to the poor dispersibility of the layered BN, which failed to fully exert its barrier function. In contrast, the modified BN significantly improves its dispersibility and barrier capability in the BNOH@PDA/EP coating. Consequently, only minor corrosion traces were observed after 14 days exposure (Fig. S12c), and its corrosion resistance still outperforms both the pure EP coating and the BN/EP coating even after 28 days of exposure (Fig. 6c). The BNOH@PDA-Ce-MOFs/EP coating demonstrates the least amount of corrosion products throughout 28 days salt spray test (Fig. 6d and S12d), maintaining a relatively clean surface with significantly reduced corrosion products. These results indicate that the modification of BNOH@PDA-Ce-MOFs by PDA and 2-methylimidazole further enhances the dispersibility and barrier capability of BN. Moreover, the synergistic effect between the corrosion inhibition of Ce-MOFs and the barrier function of BN significantly improves the long-term corrosion resistance of the coating.

To further investigate the corrosion inhibition behavior of BNOH@PDA-Ce-MOFs/EP coating and its protective mechanism, the coatings with artificial scratches were immersed in 3.5 wt.% NaCl solution. As shown in Fig. 7a-d, after 1 h of immersion, the scratches on the EP and BN/EP coatings become wider, indicating that corrosion begin to occur around the scratches. In contrast, the traces at the BNOH@PDA/EP coating and BNOH@PDA-Ce-MOFs/EP coating only slight change, and the metal substrate has not yet undergone changes. After 48 h immersion, besides BNOH@PDA-Ce-MOFs, the scratches of the other coatings all had been enlarged and corrosion of substrate become seriously. The BNOH@PDA-Ce-MOFs/EP coating with artificial scratches was immersed in 3.5 wt.% NaCl for 48 h. After immersion, the surface was washed with deionized water, dried, and characterized by SEM/EDS. As shown in Fig. S13, a passivation film was formed at the scratch sites. EDS results showed that the film consists mainly of Fe, O, and Ce, indicating that Ce ions released from the BNOH@PDA-Ce-MOFs can form a cerium-containing passivation film in corrosive environment, thereby preventing the metal from further corrosion. In addition to the physical barrier of BN on corrosion, the other reason is that the Ce ions in the BNOH@PDA-Ce-MOFs/EP coating could be released to form a passivation film, preventing the corrosion from metal substrate, when the corrosive medium reacted with the metal around the scratch area.

It is important to measure the adhesion of wet and dry coatings simultaneously to access coating durability and environmental resistance. The dry and wet adhesion results of all samples are shown in Fig. S14. Under dry condition, the adhesion strength of pure EP coating is less than 3.2 MPa. In contrast, the adhesion strength increases considerably with addition of BN (3.5 MPa), BNOH@PDA (5.6 MPa), Ce-MOFs (5.2 MPa), and BNOH@PDA-Ce-MOFs (6.2 MPa). This is due to that the fillers decrease the coating defects and improve the dry adhesion of the coating. After immersing all coatings in 5.0 wt.% NaCl solution for 7 days, the adhesion of EP coating is 2.1 MPa while the adhesion of BN/EP, BNOH@PDA/EP, Ce-MOFs/EP, and BNOH@PDA-Ce-MOFs/EP composite coatings respectively is 2.8, 3.7, 3.4, and 4.0 MPa. Consequently, BNOH@PDA, Ce-MOFs, and BNOH@PDA-Ce-MOFs fillers have effectively decreased coating pores in epoxy, which improves the antistripping ability of EP coating.

Figure 8 schematically illustrates the corrosion inhibition mechanism of coatings. In the case of the pure EP coating (Fig. 8a), its inherent defects and pores allow corrosive media ($O_2$, $H_2O$, $Cl^-$) easily penetrate from the coating to reach the metal substrate, leading to severe corrosion (Ref 44). As for the BN/EP coating (Fig. 8b), although BN could bring a physical barrier effect by prolonging the diffusion path of corrosive species, the poor dispersion of BN in the coating limits the influence on enhancing the corrosion resistance (Ref 21). In the BNOH@PDA/EP coating, the improved dispersion of modified BN significantly delays the corrosion process and enhances the corrosion resistance of coating. The BNOH@PDA-Ce-MOFs/EP coating demonstrates exceptional corrosion inhibition performance, primarily attributing to the synergistic effects of PDA and 2-methylimidazole, which promotes uniform BN distribution, blocks inherent defects and pores of coating, and further extends the diffusion path of corrosive media, thereby endowing the coating with superior barrier properties. Additionally, $Ce^{3+}$ ions in the Ce-MOFs can form a passivation layer composed of cerium hydroxide or cerium oxide on the metal substrate, providing an additional corrosion inhibition effect. Consequently, the physical barrier effect of BN and the corrosion inhibition properties of Ce-MOFs synergistically enhance the long-term corrosion resistance of the coating.

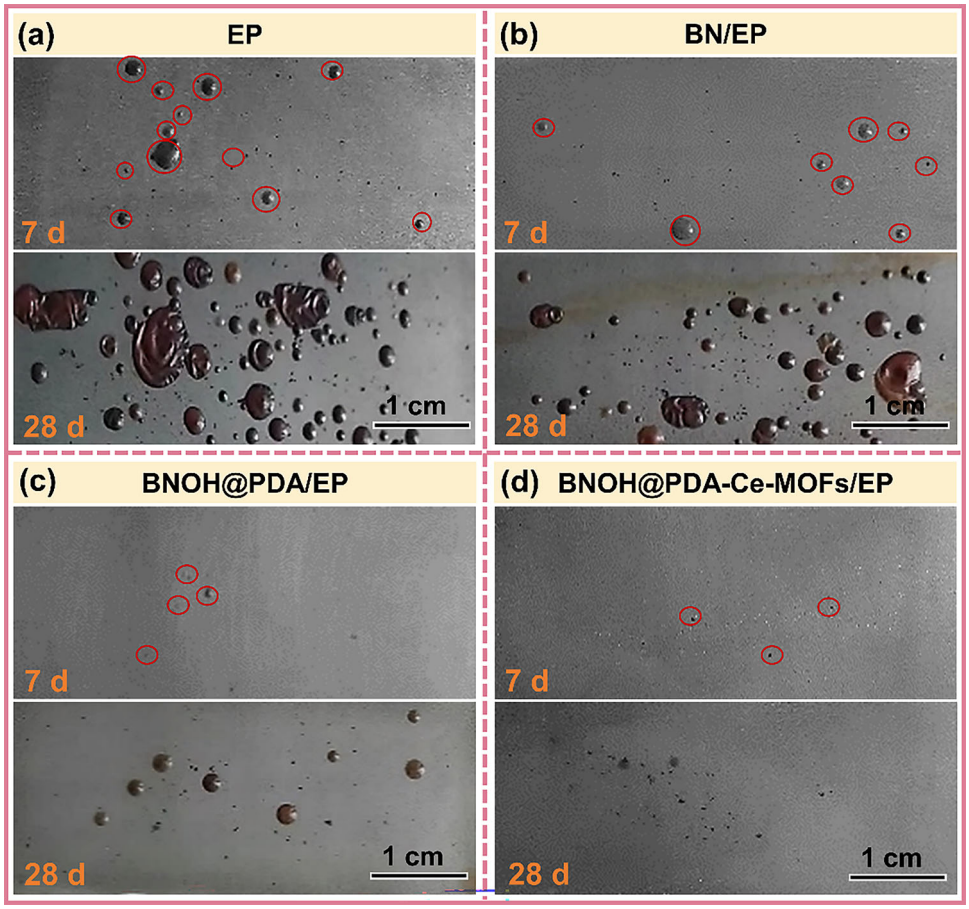


**Fig. 6** Optical images of (a) EP, (b) BN/EP, (c) BNOH@PDA/EP, and (d) BNOH@PDA-Ce-MOFs/EP coatings after the neutral salt spray test lasting 7 days and 28 days

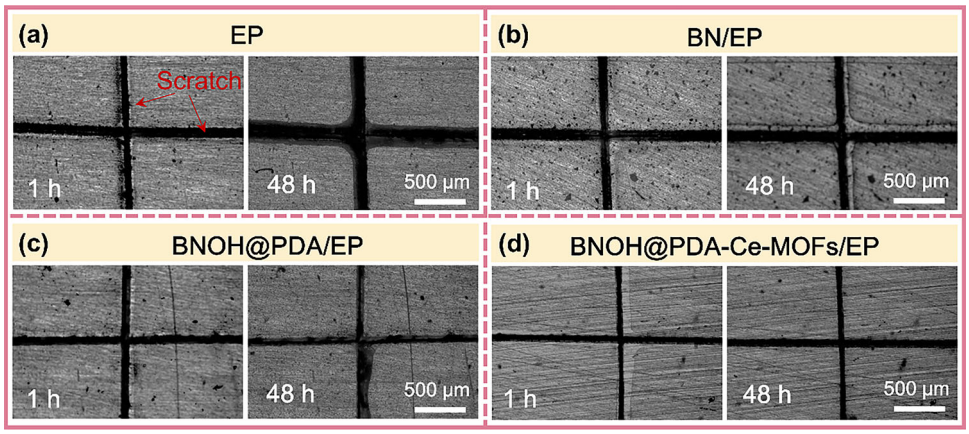


**Fig. 7** Microscopic images of scratch on the coating surface of (a) EP, (b) BN/EP, (c) BNOH@PDA/EP, and (d) BNOH@PDA-Ce-MOFs/EP coatings of immersing in 3.5 wt.% NaCl solution

## 4. Conclusion

In summary, two-dimensional BN nanosheets were hydroxylated to get BNOH with good dispersibility, on which Ce-MOFs were uniformly deposited through PDA interaction and thus produced BNOH@PDA-Ce-MOFs nanocomposite. The nanocomposite was successfully used as filler for the preparation of anticorrosion coating. The results showed that as nanofiller for epoxy coating, BNOH@PDA-Ce-MOFs effectively reduced inherent defects and pores in the coating. Moreover, the superior barrier properties of BNOH@PDA-Ce-MOFs prolonged the diffusion path of corrosive media, significantly delaying corrosion process. Meanwhile, the corrosion inhibition effect that a dense passivation film of cerium hydroxide or cerium oxide resulted by Ce-MOFs on the surface of the metal substrate, effectively suppresses the cathodic

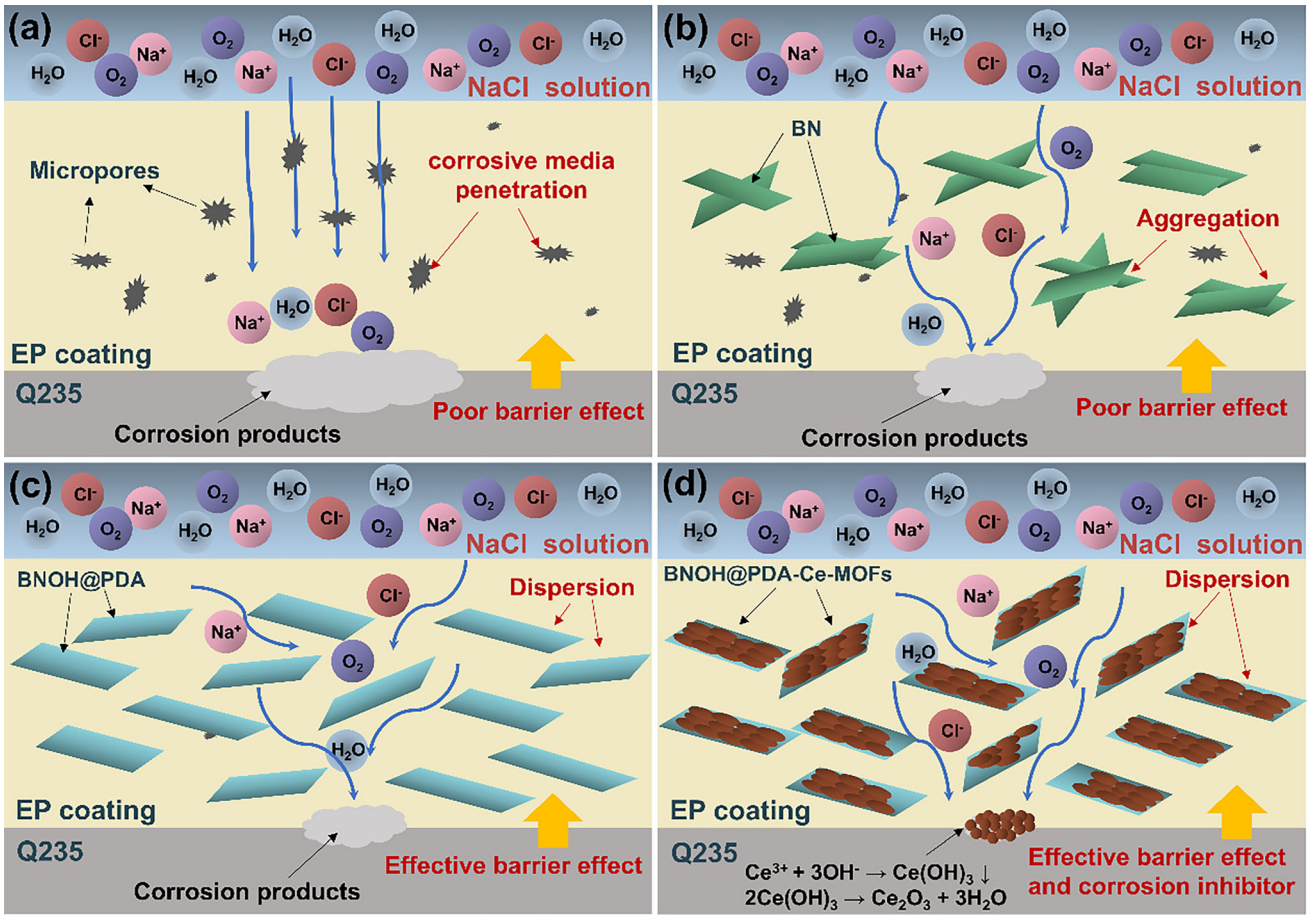


**Fig. 8** Schematic diagram of anti-corrosion mechanism of coating (a) EP, (b) BN/EP, (c) BNOH@PDA/EP, and (d) BNOH@PDA-Ce-MOFs/EP

reduction reactions and interfacial charge transfer, further enhancing the anti-corrosion capability of the coating. The salt spray tests further verified the long-term stability and reliability of the BNOH@PDA-Ce-MOFs/EP coating under harsh conditions.

## Acknowledgements

This work was supported by the National Natural Science Foundation of China, No.50801035, the Startup Fund for Doctoral Research of Liaoning (2023-BS-184), and the Fundamental Research Funds for the Liaoning Universities (LJ222410146062, LJ212410146075).

## Author Contributions

Yanqiu Zhang: conceptualization, methodology, investigation, writing; Hongwei Zhao: formal analysis and data curation; Zhaowen Tian: methodology and data curation; Zheyan Tang: methodology and data curation; Ruiyu Ma: data curation and investigation; Qingdong Li: Formal analysis and investigation; Xueyuan Zhang: Formal analysis and investigation; Lixiang Li: writing—review and editing and supervision; Baigang An: writing – review and editing, funding acquisition, and supervision.

## Data Availability

The data that support the findings of this study are available from the corresponding author upon reasonable request.

## Conflict of interest

There are no conflicts to declare.

## References

1. S. Wang, Z. Hu, J. Shi, G. Chen, Q. Zhang, Z. Weng, K. Wu, and M. Lu, Green Synthesis of Graphene with the Assistance of Modified Lignin and its Application in Anticorrosive Waterborne Epoxy Coatings, *Appl. Surf. Sci.*, 2019, **484**, p 759–770. https://doi.org/10.1016/j.apsusc.2019.03.229
2. Y. Ma, Y. Ye, H. Wan, L. Chen, H. Zhou, and J. Chen, Chemical Modification of Graphene Oxide to Reinforce the Corrosion Protection Performance of UV-Curable Polyurethane Acrylate Coating, *Prog. Org. Coat.*, 2020, **141**, p 105547–105557. https://doi.org/10.1016/j.porgcoat.2020.105547
3. L. Guo, H. Wang, X. Li, G. Fei, Y. Yuan, and Y. Li, A Synergistic System of Polyaniline@ Graphene-Alkyd Resin via a Gemini Surfactant for Enhanced Anti-Corrosion Properties, *Prog. Org. Coat.*, 2022, **170**, p 106944–106955. https://doi.org/10.1016/j.porgcoat.2022.106944
4. B. Zhang, H. Fan, W. Xu, and J. Duan, Thermally Triggered Self-Healing Epoxy Coating Towards Sustained Anti-Corrosion, *J. Mater. Res. Technol.*, 2022, **17**, p 2684–2689. https://doi.org/10.1016/j.jmrt.2022.02.041

5. Q. Li, C.E. Weinell, and S. Kiil, Detection and Quantification of Premature Crack Formation in Curing Epoxy Coatings, *Ind. Eng. Chem. Res.*, 2022, **61**(35), p 13092–13103. https://doi.org/10.1021/acs.iecr.2c01949
6. A. Diraki and S. Omanovic, Smart PANI/epoxy anti-Corrosive Coating for Protection of Carbon Steel in Sea Water, *Prog. Org. Coat.*, 2022, **168**, p 106835–106842. https://doi.org/10.1016/j.porgcoat.2022.106835
7. S. Wan, H. Chen, X. Ma, L. Chen, K. Lei, B. Liao, Z. Dong, and X. Guo, Anticorrosive Reinforcement of Waterborne Epoxy Coating on Q235 Steel Using NZ/BNNS Nanocomposites, *Prog. Org. Coat.*, 2021, **159**, p 106410–106421. https://doi.org/10.1016/j.porgcoat.2021.106410
8. M. Cui, S. Ren, J. Chen, S. Liu, G. Zhang, H. Zhao, L. Wang, and Q. Xue, Anticorrosive Performance of Waterborne Epoxy Coatings Containing Water-Dispersible Hexagonal Boron Nitride (h-BN) Nanosheets, *Appl. Surf. Sci.*, 2017, **397**, p 77–86. https://doi.org/10.1016/j.apsusc.2016.11.141
9. G. Tang, X. Hou, Y. Wang, Z. Yan, T. Ren, L. Ma, X. Huang, and C. Wang, Hexagonal Boron Nitride/Polyaniline Nanocomposites for Anticorrosive Waterborne Epoxy Coatings, *ACS Appl. Nano Mater.*, 2022, **5**(1), p 361–372. https://doi.org/10.1021/acsanm.1c03173
10. L. Zhou, P. Zhang, L. Shen, L. Chu, J. Wu, Y. Ding, B. Zhong, X. Zhang, and N. Bao, Modified Graphene Oxide/Waterborne Epoxy Composite Coating with Enhanced Corrosion Resistance, *Prog. Org. Coat.*, 2022, **172**, p 107100–107109. https://doi.org/10.1016/j.porgcoat.2022.107100
11. Y. Zhang, J. Sun, X. Xiao, N. Wang, G. Meng, and L. Gu, Graphene-Like Two-Dimensional Nanosheets-Based Anticorrosive Coatings: A Review, *J. Mater. Sci. Technol.*, 2022, **129**, p 139–162. https://doi.org/10.1016/j.jmst.2022.04.032
12. G. Cui, Z. Bi, R. Zhang, J. Liu, X. Yu, and Z. Li, A Comprehensive Review on Graphene-Based Anti-Corrosive Coatings, *Chem. Eng. J.*, 2019, **373**, p 104–121. https://doi.org/10.1016/j.cej.2019.05.034
13. G. Jena and J. Philip, A Review on Recent Advances in Graphene Oxide-Based Composite Coatings for Anticorrosion Applications, *Prog. Org. Coat.*, 2022, **173**, p 107208–107228. https://doi.org/10.1016/j.porgcoat.2022.107208
14. J. Mu, F. Gao, G. Cui, S. Wang, S. Tang, and Z. Li, A Comprehensive Review of Anticorrosive Graphene-Composite Coatings, *Prog. Org. Coat.*, 2021, **157**, p 106321–106344. https://doi.org/10.1016/j.porgcoat.2021.106321
15. M. Cui, S. Ren, S. Qin, Q. Xue, H. Zhao, and L. Wang, Processable Poly(2-butylaniline)/hexagonal Boron Nitride Nanohybrids for Synergetic Anticorrosive Reinforcement of Epoxy Coating, *Corros. Sci.*, 2018, **131**, p 187–198. https://doi.org/10.1016/j.corsci.2017.11.022
16. J. Sun, Z. Tang, G. Meng, and L. Gu, Silane Functionalized Plasma-Treated Boron Nitride Nanosheets for Anticorrosive Reinforcement of Waterborne Epoxy Coatings, *Prog. Org. Coat.*, 2022, **167**, p 106831–106838. https://doi.org/10.1016/j.porgcoat.2022.106831
17. Y. Wu, F. Jiang, Y. Qiang, and W. Zhao, Synthesizing a Novel Fluorinated Reduced Graphene Oxide-$CeO_2$ Hybrid Nanofiller to Achieve Highly Corrosion Protection for Waterborne Epoxy Coatings, *Carbon*, 2021, **176**, p 39–51. https://doi.org/10.1016/j.carbon.2021.01.135
18. S. Wu, R.B. Ladani, J. Zhang, E. Bafekrpour, K. Ghorbani, A.P. Mouritz, A.J. Kinloch, and C.H. Wang, Aligning Multilayer Graphene Flakes with an External Electric Field to Improve Multifunctional Properties of Epoxy Nanocomposites, *Carbon*, 2015, **94**, p 607–618. https://doi.org/10.1016/j.carbon.2015.07.026
19. X. Zhu, H. Zhao, L. Wang, and Q. Xue, Bioinspired Ultrathin Graphene Nanosheets Sandwiched Between Epoxy Layers for High Performance of Anticorrosion Coatings, *Chem. Eng. J.*, 2021, **410**, p 128301–128309. https://doi.org/10.1016/j.cej.2020.128301
20. Y. Su, S. Qiu, J. Wei, X. Zhu, H. Zhao, and Q. Xue, Sulfonated Polyaniline Assisted Hierarchical Assembly of Graphene-LDH Nanohybrid for Enhanced Anticorrosion Performance of Waterborne Epoxy Coatings, *Chem. Eng. J.*, 2021, **426**, p 131269–131278. https://doi.org/10.1016/j.cej.2021.131269
21. Y. Wu, Y. He, T. Zhou, C. Chen, F. Zhong, Y. Xia, P. Xie, and C. Zhang, Synergistic Functionalization of h-BN by Mechanical Exfoliation and PEI Chemical Modification for Enhancing the Corrosion Resistance of Waterborne Epoxy Coating, *Prog. Org. Coat.*, 2020, **142**, p 105541–105551. https://doi.org/10.1016/j.porgcoat.2020.105541
22. E. Songfeng, X. Ye, M. Wang, J. Huang, Q. Ma, Z. Jin, D. Ning, and Z. Lu, Enhancing the Tribological Properties of Boron Nitride by Bioinspired Polydopamine Modification, *Appl. Surf. Sci.*, 2020, **529**, p 147054–147060. https://doi.org/10.1016/j.apsusc.2020.147054
23. Q. Zhao, W. Zhao, and Y. Wu, Constructing Bi-Functional Ce-MOF on Carbon Fiber Endowing Epoxy Coating with Excellent Anti-Corrosion and Erosion Wear Resistance, *Carbon*, 2023, **214**, p 118374–118387. https://doi.org/10.1016/j.carbon.2023.118374
24. M. He, L. Wang, Y. Lv, X. Wang, J. Zhu, Y. Zhang, and T. Liu, Novel Polydopamine/Metal Organic Framework thin Film Nanocomposite Forward Osmosis Membrane for Salt Rejection and Heavy Metal Removal, *Chem. Eng. J.*, 2020, **389**, p 124452–124465. https://doi.org/10.1016/j.cej.2020.124452
25. N. Keshmiri, P. Najmi, M. Ramezanzadeh, and B. Ramezanzadeh, Designing an eco-friendly lanthanide-based Metal Organic Framework (MOF) Assembled Graphene-Oxide with Superior Active Anti-Corrosion Performance in Epoxy Composite, *J. Cleaner Prod.*, 2021, **319**, p 128732–128746. https://doi.org/10.1016/j.jclepro.2021.128732
26. Y. Lv, J. Zhao, B. Fan, H. Murtaza, J. Wang, W. Jing, and L. Chao, Designing a High Barrier, Tough and Self-Repairing Epoxy Composite Coatings with Ce-MOF Decorated 2D α-ZrP Smart Nanofiller, *Corros. Sci.*, 2024, **237**, p 112338–112355. https://doi.org/10.1016/j.corsci.2024.112338
27. M. Motamedi, M. Ramezanzadeh, B. Ramezanzadeh, and M. Mahdavian, One-Pot Synthesis and Construction of a High Performance Metal-Organic Structured Nano Pigment Based on Nanoceria Decorated Cerium (III)-Imidazole Network (NC/CIN) for Effective Epoxy Composite Coating Anti-Corrosion and Thermo-Mechanical Properties Improvement, *Chem. Eng. J.*, 2020, **382**, p 122820–122832. https://doi.org/10.1016/j.cej.2019.122820
28. X. Li, Y. Di, Z. Chen, and W. Yang, pH-Responsive Bimetallic Ce-ZIF-8 Nanocontainer for the Active Corrosion Protection of Al Alloys, *Colloids Surf. A Physicochem. Eng. Aspects*, 2022, **653**, p 129990–130001. https://doi.org/10.1016/j.colsurfa.2022.129990
29. X. Zhang, B. Li, T. Chen, X. Ke, and R. Xiao, Study on $CePO_4$ Modified PANI/RGO Composites to Enhance the Anti-Corrosion Property of Epoxy Resin, *Prog. Org. Coat.*, 2023, **178**, p 107472–107486. https://doi.org/10.1016/j.porgcoat.2023.107472
30. S. Xiao, X. Cao, Z. Dong, X. Ma, X. Zhang, and G. Cai, A pH-Responsive Cerium-Imidazole Decorated ZIF-8 to Achieve Self-Healing Barrier Property for Epoxy Coating on Al Alloy by Controlled Release, *Prog. Org. Coat.*, 2022, **163**, p 106640–106651. https://doi.org/10.1016/j.porgcoat.2021.106640
31. M. Ramezanzadeh, B. Ramezanzadeh, M. Mahdavian, and G. Bahlakeh, Development of Metal-Organic Framework (MOF) Decorated Graphene Oxide Nanoplatforms for Anti-Corrosion Epoxy Coatings, *Carbon*, 2020, **161**, p 231–251. https://doi.org/10.1016/j.carbon.2020.01.082
32. H. Li, Q.H. Zhang, X.Z. Meng, P. Liu, L.K. Wu, and F.-H. Cao, A Novel Cerium Organic Network Modified Graphene Oxide Prepared Multifunctional Waterborne Epoxy-Based Coating with Excellent Mechanical and Passive/Active Anti-Corrosion Properties, *Chem. Eng. J.*, 2023, **465**, p 142997–143009. https://doi.org/10.1016/j.cej.2023.142997
33. N. Shi, H. Li, X. Li, H. Luo, J. Jin, J. Wang, and S. Li, ZIF-8 and Benzimidazole Co-Modified h-BN for Enhancing Anti-Corrosion Performance of Epoxy Coatings, *Prog. Org. Coat.*, 2023, **183**, p 107808–107819. https://doi.org/10.1016/j.porgcoat.2023.107808
34. Z. Yang, G. Xiao, C. Chen, C. Chen, M. Wang, F. Zhong, S. Zeng, and L. Lin, Synergistic Decoration of Organic Titanium and Polydopamine on Boron Nitride to Enhance Fire Resistance of Intumescent Waterborne Epoxy Coating, *Colloids Surf. A Physicochem. Eng. Aspects*, 2021, **621**, p 126561–126577. https://doi.org/10.1016/j.colsurfa.2021.126561
35. C. Bai, F. Wang, Z. Zhao, B. Zhang, Y. Yu, and J. Zhang, Mussel-Inspired Facile Fabrication of Dense Hexagonal Boron Nitride Nanosheet-Based Coatings for Anticorrosion and Antifriction Applications, *Mater. Today Nano*, 2021, **15**, p 100129–100142. https://doi.org/10.1016/j.mtnano.2021.100129
36. Y. Xue, J. Shao, G. Sui, Y. Ma, and H. Li, Rapid Detection of Orange II Dyes in Water with SERS Imprinted Sensor Based on PDA-Modified MOFs@Ag, *J. Environ. Chem. Eng.*, 2021, **9**(6), p 106317–106324. https://doi.org/10.1016/j.jece.2021.106317
37. J. Yang, K. Li, C. Li, and J. Gu, Intrinsic Apyrase-like Activity of Cerium-Based Metal-Organic Frameworks (MOFs): Dephosphoryla-

tion of Adenosine Tri- and Diphosphate, *Angew. Chem. Int. Ed.*, 2020, **59**(51), p 22952–22956. https://doi.org/10.1002/anie.202008259

38. J. Wang, J. Zhao, M. Tabish, F. Shi, B. Fan, L. Peng, and Q. Cheng, Intelligent Anticorrosion Coating Based on Mesostructured BTA@m-$CeO_2$/g-$C_3N_4$ Nanocomposites for Inhibiting the Filiform Corrosion of Zn-Mg-Al Coated Steel, *Corros. Sci.*, 2023, **221**, p 111331–111347. https://doi.org/10.1016/j.corsci.2023.111331
39. M. Zhou, C. Zhao, P. Liu, and H. Yu, Adsorption Behavior of $Ti_3C_2Tx$ with h-BN Nanosheet and their Application in Waterborne Epoxy Anti-Corrosion Coating, *Appl. Surf. Sci.*, 2022, **586**, p 152778–152788. https://doi.org/10.1016/j.apsusc.2022.152778
40. L. Yi, S. Song, and Y. Liu, Fabrication of Functionalized Boron Nitride Modified Self-Healing Composite Coating for Corrosion and Wear Protection, *Compos. A*, 2025, **191**, p 108747–108759. https://doi.org/10.1016/j.compositesa.2025.108747
41. M. Mirzaee, A. Rashidi, A. Seif, P.L. Silvestrelli, S. Pourhashem, M.S. Gohari, and J. Duan, Amino-Silane co-Functionalized h-BN Nanofibers with Anti-Corrosive Function for Epoxy Coating, *React. Funct. Polym.*, 2022, **174**, p 105244–105256. https://doi.org/10.1016/j.reactfunctpolym.2022.105244
42. Y. Fen, J. Han, K. Liu, L. Ren, H. Zhang, and J. Chen, Noncovalently Functionalized Hexagonal Boron Nitride Nanosheets of Poly(m-Aminophenol) by Enhanced Corrosion Protection of Epoxy Coating, *Surf. Interfaces*, 2025, **65**, p 106391–106401. https://doi.org/10.1016/j.surfin.2025.106391
43. S. Ren, F. Meng, X. Li, Y. Cui, R. Liu, Y. Liu, X. Hu, L. Liu, and F. Wang, A Self-Healing Epoxy Composite Coating Based on pH-Responsive PCN-222 Smart Containers for Long-Term Anticorrosion of Aluminum Alloy, *Corros. Sci.*, 2023, **221**, p 111318–111331. https://doi.org/10.1016/j.corsci.2023.111318
44. S. Wan, H. Chen, G. Cai, B. Liao, and X. Guo, Functionalization of h-BN by the Exfoliation and Modification of Carbon Dots for Enhancing Corrosion Resistance of Waterborne Epoxy Coating, *Prog. Org. Coat.*, 2022, **165**, p 106757–106766. https://doi.org/10.1016/j.porgcoat.2022.106757